Nickel nanoparticles immobilized on pristine halloysite: an outstanding catalyst for hydrogenation processes

Alejandro Pérez Alonso, Steven Mauriés, Jean-Bernard Ledeuil, Lénaïc Madec, Doan Pham Minh, Daniel Pla, Montserrat Gómez

ChemCatChem

Research Article
doi.org/10.1002/cctc.202200775

Chemistry Europe
European Chemical Societies Publishing

www.chemcatchem.org

Nickel Nanoparticles Immobilized on Pristine Halloysite: An Outstanding Catalyst for Hydrogenation Processes

Alejandro Pérez Alonso,[a, b] Steven Mauriés,[a] Jean-Bernard Ledeuil,[c] Lénaïc Madec,[c] Doan Pham Minh,[b] Daniel Pla,*[a] and Montserrat Gómez*[a]

Nickel nanoparticles (NiNPs) immobilized on halloysite-based supports were straightforwardly synthesized and fully characterized by different techniques with the purpose of evaluating the catalytic performance of these as-prepared composite materials as catalysts in hydrogenation reactions. Thus, halloysite bearing amino (HAL-NH_2) and ammonium (HAL-NEt_3) groups led to less active catalytic materials in comparison with unfunctionalized halloysite supports, probably due to relative strong metal-support interactions with amino and tetraalkylammonium functions, consequently hindering the interaction of unsaturated substrates at the surface of the catalytic material. Despite NiNPs supported on pristine halloysite provided merely agglomerates, NiNPs stabilized by quinidine on unfunctionalized halloysite (**NiC**) proved to be a highly effective and versatile catalyst operating at relative low temperature (25–100 °C) and metal loading (1–20 mol%Ni), very well-adapted to reduce a large range of functions (alkenes, alkynes, ketones, aldehydes, nitro…). Moreover, **NiC** was able to selectively reduce substrates from biomass to yield high value-added products, such as squalane, saturated fatty acids, furfuryl alcohol and γ-valerolactone.

Introduction

Clay minerals represent one of the basic constituents of soil.[1] Because of their abundance and environmental compatibility, clays have been intensely explored as catalysts, in particular applied in organic synthesis (for selected reviews, see:[2]).

Among them, halloysite (HAL), a 1:1 aluminosilicate clay, exhibits a hollow nanotubular morphology, with a general composition of $Al_2(OH)_4Si_2O_5{\cdot}nH_2O$. Depending on the source and purification treatments, the nanotubes show external and internal diameters in the range of 40–60 nm and 10–15 nm, respectively, with lengths comprised between 500–1500 nm, where each nanotube is constituted of *ca.* 10–15 aluminosilicate layer rolls; these layers are assembled by hydrogen bonds (between octahedral $Al(OH)_6$ and tetrahedral SiO_4 sites), resulting in hollow nanotubes featuring inner alumina-rich domains and outer silica enriched surface areas.[3] Because of its availability, biocompatibility and adjustable characteristics, such as a high surface area and easy chemical surface modification, HAL has found applications in a wide range of fields, including drug delivery, energy storage, and environmental remediation among others,[4] and also in catalysis.[5] Actually, halloysite has been efficiently applied as acid-based catalyst for organic transformations such as cyclo-condensation of chiral alcohols with ketones[6] and esterification of carboxylic acids from biomass.[7] HAL can be easily functionalized through the reactivity of silanol and/or aluminol groups, mainly using organosilanes.[8] This fact together with its nanotubular structure and physico-chemical properties renders HAL appropriate for the immobilization of metal-based nanoparticles (MNPs).[9] Thus, gold nanoparticles were immobilized on decorated HAL with polyethylenimine and applied for the selective oxidation of benzyl alcohol into benzaldehyde.[10] PdNi and PdCo bimetallic nanoparticles were immobilized on HAL for methane oxidation, giving exclusively carbon dioxide and water.[11] Regarding metal-catalyzed hydrogenations, MNPs based on heavy metals (Ru, Rh, Pd, Pt, Au…) exhibited quite high stability and catalytic efficiency, but showed a limited scope.[8,12] To the best of our knowledge, only one recently reported contribution describing nickel supported on HAL has been thus far applied to furfural hydrogenation.[13]

This contribution represents the first report describing well-defined Ni nanoparticles on halloysites. We describe herein the synthesis and full characterization of nickel-based nanoparticles on both functionalized and pristine halloysite-based supports and their efficient catalytic applications in hydrogenations of a

[a] *A. Pérez Alonso, S. Mauriés, Dr. D. Pla, Prof. M. Gómez*
Laboratoire Hétérochimie Fondamentale et Appliquée
UMR CNRS 5069
Université Toulouse 3 – Paul Sabatier
118 route de Narbonne
31062 Toulouse Cedex 9 (France)
E-mail: pla@lhfa.fr
montserrat.gomez-simon@univ-tlse3.fr
[b] *A. Pérez Alonso, Prof. D. Pham Minh*
Université de Toulouse
IMT Mines Albi
UMR CNRS 5302
Campus Jarlard
81013 Albi Cedex 9 (France)
[c] *J.-B. Ledeuil, Dr. L. Madec*
Université de Pau et des Pays de l'Adour
E2S UPPA
CNRS, IPREM
64053 Pau (France)

Supporting information for this article is available on the WWW under https://doi.org/10.1002/cctc.202200775

large variety of functional groups (alkynes, alkenes, ketones, aldehydes, and nitro groups), including the hydrogenation of substrates leading to the formation of added value products from bio-mass reactants, such as squalane, saturated fatty acids, furfuryl alcohol and γ-valerolactone.

Results and Discussion

Synthesis and characterization of NiNPs on halloysite-based supports. With the aim of modifying the support surface with functional groups able to stabilize metal nanoparticles, we prepared both HAL-NH_2 (based on the methodology described in the literature),[8] as well as a novel functionalized halloysite bearing ammonium moieties, HAL-NEt_3, thus favoring the NiNPs stabilization by coordination and electrostatic effects, respectively (Figure 1a). These supports were characterized by ICP-AES (Inductively coupled plasma atomic emission spectroscopy), elemental analysis, FTIR (Fourier Transform Infrared spectroscopy) and ssNMR (solid state Nuclear Magnetic Resonance). FTIR spectra of HAL-NH_2 and HAL-NEt_3 showed absorption bands corresponding to CH_2 (*ca.* 1380 and 1490 cm^{-1}) and NH_2 for HAL-NH_2 (1556 cm^{-1}) deformations (see Figure S1 in the Supporting Information); for the hydroxyl groups, no significant variations were observed (3500–3600 cm^{-1}), in agreement with the partial functionalization of the as-prepared supports (see below). ^{29}Si CP/MAS NMR spectra of commercial halloysite, HAL-NH_2 and HAL-NEt_3 exhibited a chemical shift at *ca.* −92 ppm assigned to the Q^3 band of halloysite [$(Si(OSi)_3(OAl)]$; for HAL-NH_2 and HAL-NEt_3, two bands at *ca.* −59 ppm and −68 ppm were also observed which can be attributed to bidentate (T^2) and tridentate (T^3) bonded Si, respectively, meaning that two or three ethoxy groups from the starting material were hydrolyzed as shown schematically in Figure 1 (see Figure S2A in the Supporting Information).[14] This behavior was also corroborated by ^{13}C CP/MAS NMR spectra of HAL-NH_2 and HAL-NEt_3, showing clearly the resonances corresponding to the propyl-amino and propyl-triethylammonium groups, respectively, in the absence of the diagnostic signals of ethoxy groups (see Figure S3 in the Supporting Information). These observations agree with the CHN elemental analyses of HAL-NH_2 and HAL-NEt_3. Thus, the C/N ratios for HAL-NH_2 and HAL-NEt_3, 3.2 and 8.75 respectively, are higher than the expected ratios for the completely hydrolyzed γ-aminopropyltriethoxysilane molecular precursors (2.7 and 6, respectively), corroborating the partial hydrolysis of ethoxy groups (see Table S1 in the Supporting Information). ^{27}Al MAS NMR spectra for HAL and for functionalized materials HAL-NH_2 and HAL-NEt_3 did not exhibit significant differences, proving that no functionalization on aluminol moieties took place (see Figure S2B in the Supporting Information). XPS (X-ray Photoelectron Spectroscopy) analyses also confirmed the proposed functionalization of the halloysite-based materials and evidenced the presence of iodine for HAL-NEt_3 (see Figure S4 in the Supporting Information).

The synthesis of NiNPs supported on (un)functionalized halloysite was carried out under relatively mild conditions, using nickel bis(cyclooctadiene) as metal precursor in ethanol under hydrogen atmosphere at 100 °C overnight (Figure 1b). When unfunctionalized **HAL** (commercial material employed without any treatment prior to its use as catalyst support), only aggregates were obtained (Figure 2a). However, using HAL-NH_2 as both support and NPs stabilizer, gave both supported and

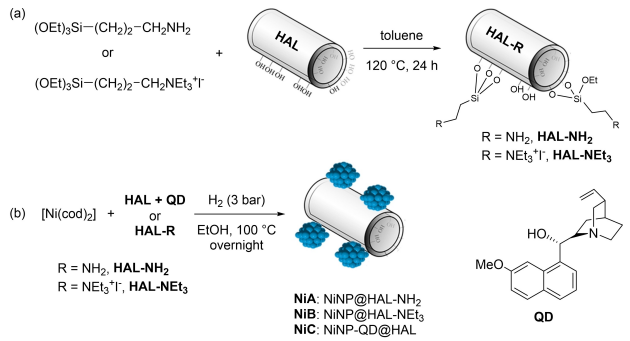

Figure 1. (a) Synthesis of functionalized halloysites (**HAL-NH_2** and **HAL-NEt_3**); (b) one-pot synthesis of NiNPs supported on HAL-based materials, **NiA**–**NiC** (blue clusters denote NiNPs).

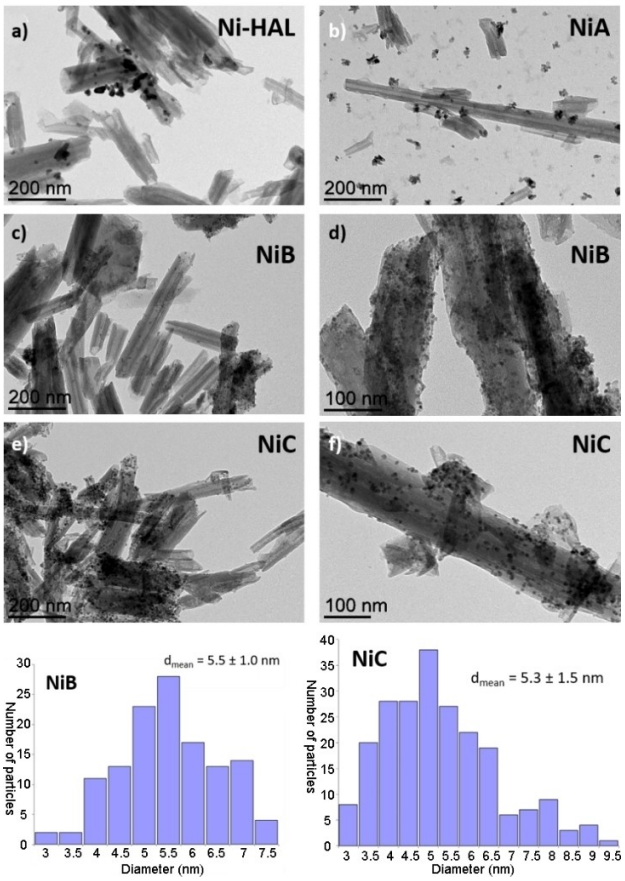

Figure 2. TEM micrographs of: (a) Nickel supported on HAL; (b) NiNPs supported on HAL-NH_2 (**NiA**); (c, d) NiNPs supported on HAL-NEt_3 (**NiB**); and (e, f) NiNPs supported on HAL stabilized by quinidine (**NiC**).

unsupported aggregates (Figure 2b). For HAL-NEt_3, well-dispersed spherical NiNPs on the functionalized support were obtained, exhibiting a mean diameter of 5.5 ± 1.0 nm as evidenced by TEM (Transmission Electron Microscopy; Figure 2c and 2d). The CHN elemental analysis of **NiA** and **NiB** were unchanged compared to the functionalized supports (HAL-NH_2 and HAL-NEt_3 respectively), proving that no degradation of the functionalized supports occurred during the synthesis of the catalytic materials (Figure 1b; see Table S1 in the Supporting Information).

Based on our previous experience regarding the synthesis of unsupported metal nanoparticles,[15] we added quinidine in the reaction mixture, a natural alkaloid able to stabilize MNPs,[16] also obtaining small (5.3 ± 1.5 nm) and very well-dispersed nanoparticles on unfunctionalized halloysite (Figure 2e and 2f). HAADF-STEM (High-Angle Annular Dark-Field- Scanning Transmission Electron Microscopy) coupled to EDX (Energy-Dispersive X-ray spectroscopy) analyses of **NiC** evidenced that nickel was homogenously dispersed on the support (Figure 3). However, the use of choline chloride as stabilizer led to NiNPs not adsorbed on the nanostructured clay (see Figure S5 in the Supporting Information).

ICP-AES data proved that nickel was quantitatively adsorbed on the solid (4.8 wt% for **NiA**; 5.2 wt% for **NiB**; 4.4 wt% for **NiC**). Powder X-Ray Diffraction (PXRD) of **NiC** revealed the presence of crystalline fcc Ni(0); for **NiA** and **NiB**, amorphous material was observed (broad signals), hardly distinguishing the signals corresponding to the metal phase (see Figure S6 in the Supporting Information). This fact can be due to the physisorption of (3-aminopropyl)triethoxysilane for **NiA** and 3-(triethylammonium)propyl)triethoxysilane iodide for **NiB**, in agreement with thermogravimetric analyses (Figure 4), which both materials showed a relative high mass loss in the temperature range of 70–110 °C (3.5 wt% for **NiA** and 1.9 wt% for **NiB**) in comparison with **NiC** (0.8 wt%). A comparison of PXRD diffractograms of the corresponding functionalized halloysite supports (HAL-NH_2 and HAL-Et_3, see Figure S6 in the Supporting Information), indicates that the broad signals observed at *ca.* 10–20° (2θ values) mainly appeared during the immobilization of the Ni-based nanoparticles.

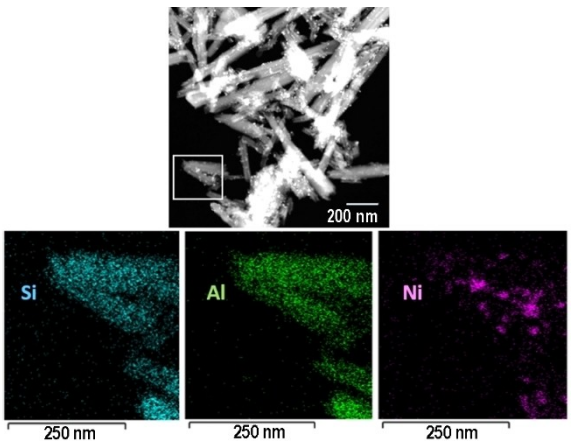

Figure 3. (a) HAADF-STEM image of **NiC** (framed area corresponding to the EDX mapping); (b) EDX mapping of **NiC**.

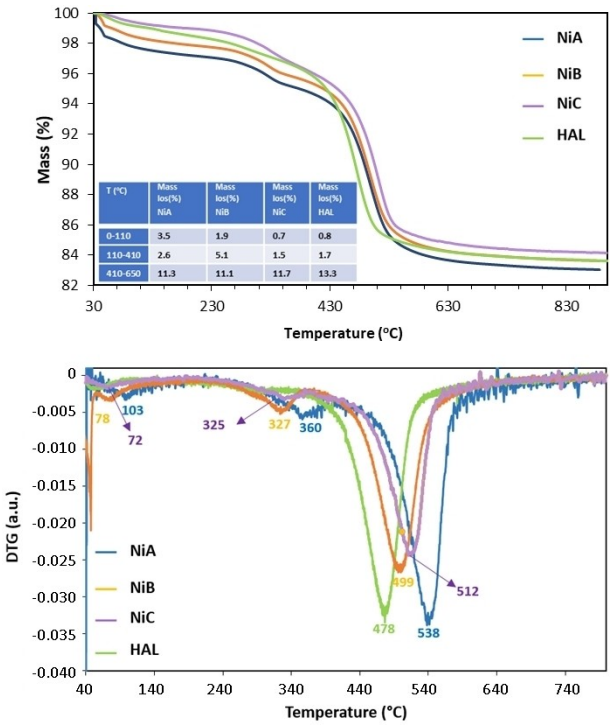

Figure 4. Thermogravimetric analyses and the corresponding derivative mass loss curves for the catalytic materials **NiA**, **NiB** and **NiC**, and halloysite (HAL).

Thermogravimetric analyses (TGA) of **NiA**, **NiB** and **NiC** showed a mass loss (0.7-3.5 %) in the temperature range of 74–110 °C, attributed to the physically adsorbed water or 3-aminopropyltriethoxysilane molecular precursors (**NiA** exhibited the highest mass loss probably due to the presence of adsorbed 3-aminopropyltriethoxysilane), in agreement with reported functionalized halloysites.[14b] These catalytic materials also showed a mass loss (1.5–5.1 %) in the temperature range of 325–360 °C, attributed to the degradation of grafted organic fragments. The third mass loss (11–11.7 %) in the temperature range of 400–650 °C, also present for pristine halloysite (13.3 % mass loss), matched with the dehydroxylation of aluminol/silanol groups (Figure 4).[14b] From these data, *ca.* 1.5–5.0 wt% of functionalization can be proposed for the three catalytic materials.

XPS survey spectrum (Figure 5, left) of **NiC** showed the presence of Ni, and Si and Al from HAL as well as N and C from quinidine (oxygen content comes from both support and stabilizer; see Table S2 in the Supporting Information for XPS at.% quantification). Note that Si, Al and O contents are in good agreement with the $Al_2(OH)_4Si_2O_5$ composition (percentage of quinidine is much lower compared to the support). Importantly, the Ni 2p XPS core level spectrum (Figure 5, right) of **NiC** showed three contributions: Ni^0 (31 %), NiO (43 %) and $Ni(OH)_2$ (26 %). These results highlight that the preparation method for **NiC** is effective to obtain zero-valent NiNPs, albeit its partial

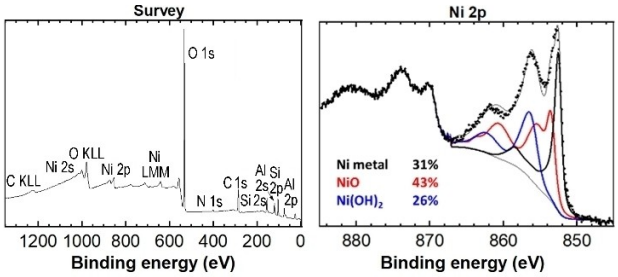

Figure 5. XPS survey (left) and Ni 2p (right) spectra of **NiC**. Black, red and blue peaks correspond to the Ni(0), NiO and $Ni(OH)_2$ envelopes (see Figure S7 and Table S2 in the Supporting Information for more information about the fit procedure) used to fit the experimental data (dotted line).

oxidation. It is important to mention that due to the low nickel content in the sample (1 at.%) and the high reactivity of the zero-valent NiNPs (rapid oxidation even under glovebox Ar atmosphere or under ultra-high vacuum during XPS analysis), XPS analysis of such powder sample was a challenge.[17] Consequently, the real percentage of Ni^0 in the sample is more likely higher that the determined one (31 %). When XPS analysis was carried out under common conditions (preparation of the sample in air), only nickel oxide was observed (see Figure S8 in the Supporting Information).

We were also interested in studying the robustness of the stabilizer under hydrogen conditions. Based on our previous work concerning the stabilization of palladium nanoparticles by cinchona derivatives,[18] we carried out a hydrogenation reaction of quinidine using **NiC** as catalyst, proving that the quinoline group was not modified in contrast to the vinyl moiety that was converted into an ethyl group (see Figure S9 in the Supporting Information); this result shows that the interaction of the stabilizer at the metal surface through the aromatic fragment could be preserved under catalytic hydrogenation conditions, in agreement with the reported works involving platinum nanoparticles.[19]

Ni-catalyzed hydrogenations. The as-prepared catalytic nanomaterials (**NiA**-**NiC**) were used for the hydrogenation of diphenylacetylene (**1**) in ethanol under smooth conditions (25 °C, 3 bar H_2, 1 mol% Ni) with the aim of comparing their catalytic activity (entries 1–3, Table 1). Nanocatalysts supported on functionalized halloysites (**NiA**, **NiB**) were less active than that on unfunctionalized support, **NiC** (entries 1 and 2 *vs* 3, Table 1). The catalyst supported on functionalized HAL with amino groups (**NiA**) was inactive after 24 h of reaction, while **NiB** led to 18% conversion to the corresponding alkene; **NiC** gave full conversion after only 7 h, selectively obtaining (*Z*)-**1 a** (entry 3, Table 1). From these results, the amino and ammonium functions on the support seem to trigger a poisoning effect probably due to strong metal-support interactions (by dative coordination of amino groups to the metal or by electrostatic interactions through the ammonium moieties), thus hindering the contact between the substrate and metal sites. Longer reaction time afforded a full hydrogenation of the exocyclic C=C, only obtaining 1,2-diphenylethane (entry 4, Table 1). For 1-phenyl-1-propyne (**2**), the hydrogenation was faster than with diphenylacetylene; thus, the selectivity towards the corresponding alkene was lower (entries 5 and 6, Table 1). In agreement with this observed behavior, **NiC** fully reduced (*Z*)-**1 a** and (*Z*)-**2 a** into **1 b** and **2 b**, respectively (entries 7 and 8, Table 1). However, lower activity was observed for the corresponding (*E*)-stereoisomers (entries 9 and 10, Table 1), without observing isomerization. The slight increase in catalyst activity working at a higher pressure (entry 11, Table 1) points to a lower adsorption energy for (*E*)-alkene than for (*Z*)-alkene on the metal surface.

Taking into account the high performance of **NiC** towards non-aromatic C–C multiple bonds, we expanded the hydro-

Table 1. Hydrogenation of alkynes (**1**, **2**) catalyzed by NiNP immobilized on halloysite-based supports, **NiA**-**NiC**.[a]

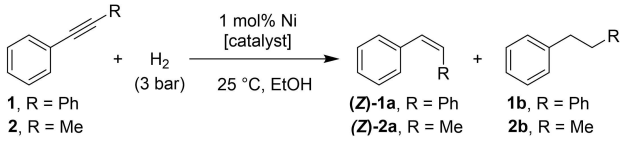

Entry	Catalyst	Substrate	t [h]	Conv. (Yield) [%][b]	Selectivity [%][b]
1	**NiA**	**1**	24	0 (0)	–
2	**NiB**	**1**	24	18 (18)	>99 (*Z*)-**1 a**
3	**NiC**	**1**	7	>99 (>99)	>99 (*Z*)-**1 a**
4	**NiC**	**1**	24	>99 (99)	99 **1 b**
5	**NiC**	**2**	3	>99 (99)	73, (*Z*)-**2 a** 27, **2 b**
6	**NiC**	**2**	6	>99 (99)	2, (*Z*)-**2 a** 98, **2 b**
7[c]	**NiC**	(*Z*)-**1 a**	24	>99 (99)	[f]
8[c]	**NiC**	(*Z*)-**2 a**	24	>99 (99)	[g]
9[d]	**NiC**	(*E*)-**1 a**	24	16 (16)	[f]
10[d]	**NiC**	(*E*)-**2 a**	24	27 (25)	[f]
11[d,e]	**NiC**	(*E*)-**1 a**	24	56 (50)	[f]

[a] Results from duplicated experiments. Reaction conditions: 1 mmol of substrate, 2 mL of degassed solvent, 0.01 mmol of total Ni (determined by ICP). [b] Determined by GC using 2-methoxynaphtalene as internal standard. [c] After 4 h, no conversion. [d] Cyclopentylmethylether (CPME) used as solvent due to the insolubility of (*E*)-**1 a** and (*E*)-**2 a** in EtOH. [e] 10 bar H_2. [f] Only **1 b** was formed. [g] Only **2 b** was formed.

genation study to other functional groups including nitro-, carbonyl- and nitrile-derivatives (Table 2). For nitroarenes (**3**–**5**), a dramatic electronic effect of the aromatic ring was observed (entries 1–3, Table 2). While nitrobenzene and 4-hydroxynitrobenzene led to the corresponding anilines in high yields (more than 80%, entries 1–2, Table 2), substrate **5** containing a chloro substituent gave a very low conversion (entry 3, Table 2), and 1,3- and 1,4-dinitrobenzene substrates were inactive. The presence of electron-withdrawing groups probably hinders the substrate coordination to the metal surface due to its lower π-electron density on the aromatic ring than those containing electron-donor moieties; in this latter case, the π-π substrate-metal surface interaction can be more favored, in agreement with the behavior observed for other types of reactivity.[20]

Aldehydes (**6**–**10**) and ketones (**11**–**15**), both bearing aryl and alkyl substituents, were efficiently reduced into the corresponding primary (entries 4–8, Table 2) and secondary alcohols (entries 9–13, Table 2), respectively. It is important to highlight that acetalization was not observed in any case (competitive reaction with ethanol), probably due to the low acidity of halloysite, in agreement with the irrelevant activity of pristine halloysite in esterification reactions compared to the high activity observed using sulfonic acid-modified HAL.[21]

The unsymmetrically substituted ketones **12**–**15** were chosen with the aim of studying the stereoselective influence of quinidine, acting as NiNP stabilizer, in the reduction towards the corresponding alcohol (entries 10–14, Table 2). For methyl phenyl ketone, isopropyl phenyl ketone and α-tetralone (**12**–**14**), only racemic mixtures were obtained (entries 10–12, Table 2; see Figure S10 in the Supporting Information). Using *rac*-**15** as substrate, a diastereomeric ratio of 44% was observed (entry 13, Table 2; see Figure S11 in the Supporting Information). With the purpose of determining the diastereoselectivity induction (promoted by the substrate structure or by the chiral stabilizer), a new Ni-based catalytic material (**NiD**) was also prepared containing an achiral stabilizer, 4-(3-phenylpropyl)pyridine, which we previously applied in the synthesis of ruthenium and palladium nanoparticles[22] (see Figure S12 in the Supporting Information). Under the same catalytic conditions, **NiD** exhibited a lower activity than **NiC** (entry 14 vs 13, Table 2), probably due to the high aggregation of NiNPs in the case of **NiD**; but both systems showed essentially the same diastereoselectivity trends, indicating that the observed behavior is induced by the substrate and not by the chiral stabilizer (see Figure S13 in the Supporting Information). Moreover, ethyl pyruvate was selectively hydrogenated, leading to a racemic mixture of ethyl lactate (entry 15, Table 2).

Benzonitrile hydrogenation led to a mixture of products, mainly constituted of *N*-benzylidenebenzylamine and dibenzylamine, together with minor amounts of benzylamine, probably due to the fast nucleophilic addition of benzylamine to the intermediate phenylmethanimine (see Figure S14 in the Supporting Information); attempts to avoid this addition by in-situ protection of benzylamine (addition of boric acid, di-tert-butyl dicarbonate or benzyl chloroformate) was unsuccessful (see Table S3 in the Supporting Information).[23]

We studied the reuse of the catalytic material **NiC** for the benzaldehyde hydrogenation. The catalyst was recycled without activity loss for 5 runs, exhibiting a slight yield decrease up to the 8th run (see Figure S15 in the Supporting Information). ICP-AES analyses of the organic extracts (after the 3rd, 7th and 8th runs) evidenced that no significant nickel leaching occurred.

Taking into account the performance of **NiC** for the reduction of C=C bonds and carbonyl groups, we were interested in the hydrogenation of substrates leading to added-value products, in particular those coming from biomass, such as fatty acids, squalene, furfural and levulinic acid, in order to reach selectively saturated fatty acids,[24] squalane,[25] furfuryl alcohol[26] and γ-valerolactone,[27] respectively.

Regarding the formation of saturated fatty acids (Table 3), we chose stearic acid, mainly applied in the

Table 2. Ni-catalyzed hydrogenation of nitro and carbonyl derivatives.[a]

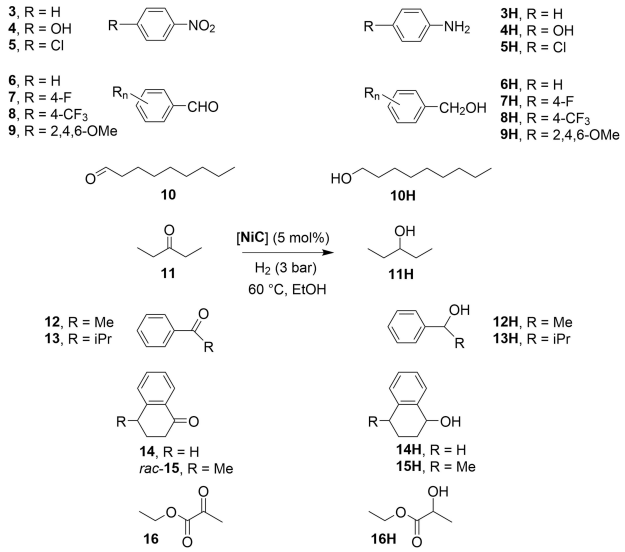

Entry	Substrate	t [h]	Conv. (Yield) [%][b]
1	**3**	4	>99 (82)[c]
2	**4**	4	>99 (99)
3	**5**	4	7 (6)
4[d]	**6**	8	82 (82)[e]
5	**7**	8	56 (54)[e]
6	**8**	8	92 (90)
7	**9**	8	86 (82)
8	**10**	8	79 (74)
9	**11**	8	>99 (87)
10	**12**	8	87 (86)
11	**13**	24	99 (99) [24 (23)][f]
12[g]	**14**	24	54 (52)
13[g]	*rac*-**15**	24	97 (87) [d.e. = 44%][j]
14[g,h]	*rac*-**15**	24	35 (33) [d.e. = 52%][j]
15	**16**	24	91 (90)

[a]Mean results from duplicated experiments. Reaction conditions: 1 mmol of substrate, 2 mL of degassed solvent, 0.05 mmol of total Ni (determined by ICP). [b] Determined by GC-FID NMR using dimethyl sulfone as internal standard. [c] 42% conversion after 2 h. [d] Using 2.5 mol% Ni. [e] Quantitative yield after 24 h. [f] Results after 8 h. [g] At 100 °C; d.e. denotes diastereomeric excess. [h] Using **NiD** as catalyst. [j] Determined by 1H NMR using dimethyl sulfone as internal standard.

Table 3. Ni-catalyzed hydrogenation of unsaturated fatty acids into stearic acid.[a]

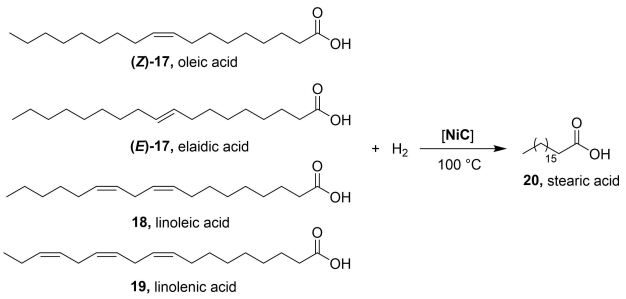

Entry	Substrate	mol% Ni	P [bar]	t (h)	Conv. (Yield) [%][b]
1	**(*Z*)-17**	10	20	8	96 (94)
2	**18**	10	20	8	73 (70)
3	**19**	10	20	8	82 (79)
4	**(*Z*)-17**	5	20	24	82 (82)
5[c]	**(*Z*)-17**	5	20	24	66 (62)[d]
6[e]	**(*Z*)-17**	10	20	8	12 (12)
7	**(*Z*)-17**	10	3	8	0
8	**(*E*)-17**	10	20	8	65 (64)

[a] Results from duplicated experiments. Reaction conditions: 1 mmol of substrate, 0.01 mmol of total Ni (determined by ICP). [b] Determined by ^{1}H NMR using dimethyl sulfone as internal standard. [c] EtOH used as solvent (2 mL). [d] Product formed correspond to ethyl stearate. [e] At 25 °C.

production of detergents, soaps and cosmetics due to both its surfactant properties and its use as food additive,[28] starting by different unsaturated acids, such as oleic [**(*Z*)-17**], elaidic [**(*E*)-17**], linoleic (**18**) and linolenic (**19**) acids. **NiC** showed a high efficiency in the hydrogenation of the C=C bonds exhibiting a (*Z*)-configuration, merely obtaining stearic acid under solvent-free conditions (entries 1–3, Table 3). Using a lower Ni loading (5 mol% Ni), the catalytic activity was moderately lower than using 10 mol% Ni (entry 4 vs entry 1, Table 3). However, a significant activity decrease was observed using ethanol as solvent, only obtaining ethyl stearate as product formed by esterification (entry 5, Table 3). Working at lower temperature or lower hydrogen pressure, the catalyst was almost inactive (entries 6 and 7, Table 3). For the hydrogenation of **(*E*)-17**, the catalytic activity decreased compared to **(*Z*)-17** (entry 8 vs 1, Table 3), in agreement with the behavior observed for the isomers of 1,2-diphenylethylene (entries 7–10, Table 1).

Squalane, an ingredient widely used in cosmetic and pharmaceutical companies for its skin moisturizer and lubricating properties,[29] was quantitatively prepared by solvent-free hydrogenation of squalene, under 40 bar H_2 pressure at 100 °C for 24 h using 20 mol% Ni (Scheme 1). This approach represents one of the few processes working under neat conditions,[30] the first involving a Ni-based catalyst; moreover, no low molecular weight alkanes coming from hydrocarbon cracking were observed. Furthermore, it is important to highlight that no nickel was detected on the isolated squalane by ICP analyses (0.1 ppm Ni after squalane extraction from the catalyst; no Ni detection after filtration through Celite). At short time, a high conversion was obtained (95%), albeit as a complex mixture of compounds due to the partial hydrogenation of squalene as

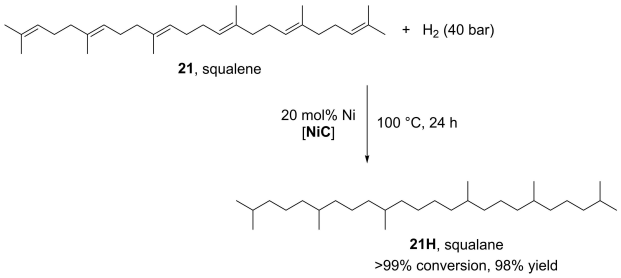

Scheme 1. Squalane formation by **NiC**-catalyzed squalene hydrogenation. Conversion and yield determined by ^{1}H NMR using 2-methoxynaphtalene as internal standard.

shown by GC analyses (see Figure S16 in the in the Supporting Information).

Moreover, we studied the selective reduction of furfural (**24**), derived from agricultural residues, to furfuryl alcohol, important compound due to its broad spectrum on industrial applications (resins, drugs, solvents, lubricants).[31] To our delight, **NiC** allowed the exclusive formation of furfuryl alcohol under smooth conditions using only 5 mol% nickel loading (entries 1–4, Table 4). Even at 25 °C for 8 h of reaction, the catalyst was active (entry 1, Table 4); at higher temperature and/or longer reaction time, high yields (>92%) were obtained (entries 2–3, Table 4), in contrast to the catalytic behavior of Raney nickel for which a mixture of products was formed without formation of furfuryl alcohol.[32] In heptane, a similar catalytic behavior was observed (entry 4 vs 2, Table 4), ruling out ethanol as a hydrogen transfer agent in these reaction conditions. Under higher H_2 pressure and temperature (20 bar H_2, 100 °C), **NiC** also hydrogenated the

Table 4. Ni-catalyzed hydrogenation of biomass substrates.[a]

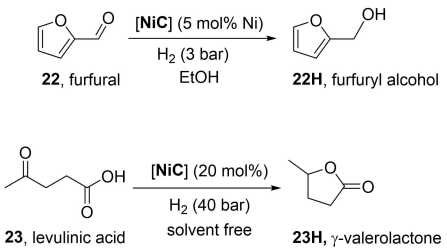

Entry	Substrate	mol% Ni	T [°C]	t [h]	P [bar]	Conv. (yield) [%][b]
1	**22**	5	25	24	3	46 (45)
2	**22**	5	60	24	3	99 (97) [66 (66)][c]
3	**22**	5	100	8	3	95 (92)
4[d]	**22**	5	60	24	3	82 (80) [59 (59)][c]
5	**22**	1	60	24	3	15 (0)[e]
6	**23**	20	100	48	40	>99 (99) [63 (52)][f]

[a] Mean results from duplicated experiments. Reaction conditions: 1 mmol of substrate, amount of total Ni determined by ICP. [b] Determined by GC-FID using 2-methoxynaphtalene as internal standard. [c] After 8 h. [d] In heptane. [e] Only acetalization was observed. [f] After 24 h.

C=C bonds of furfural, leading to a mixture of products (see Figure S17 in the Supporting Information); this result proved the higher efficiency of **NiC** compared to the Ni-based catalyst on halloysite described in the literature.[13] Using lower Ni loading (1 mol%), no formation of furfuryl alcohol was observed (entry 5, Table 4).

Levulinic acid, coming from lignocellulose exhibits an important potential as a platform chemical.[33] In particular, levulinic acid can afford γ-valerolactone by catalytic hydrogenation,[34] which is applied as green solvent, fuel additive and also for the synthesis of precursors for the production of polymers, among the most common uses.[35] Under solvent-free conditions at 100 °C and 40 bar H_2 pressure, full conversion towards γ-valerolactone was chemoselectively obtained (entry 6, Table 4); the catalyst was inactive using lower Ni loading (10 mol%) or applying lower pressure (3 bar).

Conclusion

In this work, original Ni-based catalysts supported on halloysite (a natural nanostructured clay) constituted of well-defined nanoparticles, are described for application in hydrogenation processes. Thus, we prepared composite materials constituted of nickel nanoparticles immobilized on both pure and functionalized halloysites, with the purpose of comparing their effect in catalysis. The nanomaterials were prepared by decomposition of [Ni(cod)$_2$] under a dihydrogen atmosphere in the presence of the corresponding support; the as-prepared materials were fully characterized [(HR)TEM, PXRD, XPS, FTIR, TGA, ICP], evidencing the effect of the support and added stabilizers [quinidine, choline chloride, 4-(3-phenylpropyl)pyridine] on nickel nanoparticles dispersion. Pristine halloysite in the presence of quinidine acting as NiNPs stabilizer (**NiC**) led to the most efficient and versatile catalyst, showing its performance in the reduction of several functional groups (C=C, C≡C, NO_2, carbonyl derivatives) including its ability to be reused. This catalytic material also exhibited an outstanding performance in the formation of valuable products such as saturated fatty acids, squalane, furfuryl alcohol and γ-valerolactone, from biomass substrates.

Experimental Section

Materials, instrumentation, synthesis of precursors, preparation of functionalized halloysite-based supports, and catalyst recycling are described in the Supporting Information (SI). Figures S1–S17 and Tables S1–S3 containing supplementary information in relation to that discussed in the main text; characterization of organic products obtained in the studied hydrogenations (^{1}H and ^{13}C NMR spectra, and MS data).

Synthesis of supported nickel nanoparticles on amino-functionalized halloysite (NiA: NiNP@HAL-NH_2). A Fisher-Porter bottle was charged with bis(cyclooctadiene)nickel(0) (115.0 mg, 0.42 mmol) and the functionalized halloysite HAL-NH_2 (500 mg, 1.7 mmol), and then sealed with a septum inside the glovebox. The Fisher-Porter bottle was then removed from the glovebox and the solids were suspended in degassed EtOH (20 mL) under Ar prior to sealing the Fisher-Porter with its head. The system was then pressurized with H_2 (3 bar) at room temperature, heated at 100 °C and stirred for 18 h. A black dispersion was obtained and this suspension was then transferred to a centrifuge tube under Ar. Centrifugation was carried out at 4000 rpm for 10 min. After the removal of the supernatant, the solid was dispersed in degassed EtOH (3×10 mL). The obtained black solid was dried under vacuum overnight and stored in the glovebox (420 mg, 76% yield). The as prepared catalytic material was characterized by FTIR, ICP-AES, PXRD, TGA, XPS and TEM.

Synthesis of supported nickel nanoparticles on ammonium-functionalized halloysite (NiB: NiNP@HAL-NEt_3). A Fisher-Porter bottle was charged with bis(cyclooctadiene)nickel(0) (115.0 mg, 0.42 mmol), and the functionalized halloysite material (500 mg, 1.7 mmol) and then sealed with a septum inside the glovebox. The Fisher-Porter bottle was then removed from the glovebox and the solids were suspended in degassed EtOH (20 mL) under Ar prior to sealing the Fisher-Porter with its head. The system was then pressurized with H_2 (3 bar) at room temperature, heated to 100 °C and stirred for 18 h. A black dispersion was obtained and this suspension then was transferred to a centrifuge tube under Ar. Centrifugation was carried out at 3000 rpm for 5 min. After the removal of the supernatant, the solid was dispersed in degassed EtOH (3×10 mL). The obtained black solid was dried under vacuum overnight and stored in the glovebox prior to use (460 mg, 84% yield). The as-prepared catalytic material was characterized by FTIR, ICP-AES, PXRD, TGA, XPS and TEM.

Synthesis of supported nickel nanoparticles stabilized by quinidine on unfunctionalized halloysite (NiC: NiNP-QD@HAL). A Fisher-Porter bottle was charged with bis(cyclooctadiene)nickel(0) (343.0 mg, 1.25 mmol), quinidine (QD: 371.0 mg, 1.15 mmol) and halloysite (1497 mg, 5.09 mmol), and then sealed with a septum inside the glovebox. The Fisher-Porter bottle was then removed from the glovebox and the solids were suspended in degassed EtOH (50 mL) under Ar prior to sealing the Fisher-Porter with its head. The system was then pressurized with H_2 (3 bar) at room temperature, heated at 100 °C and stirred for 18 h. A black dispersion was obtained and this suspension was then transferred to a centrifuge tube under Ar. Centrifugation was carried out at 3000 rpm for 5 min. After removal of the supernatant, the solid was dispersed in degassed EtOH (3×10 mL). The obtained black solid was dried under vacuum overnight and stored in the glovebox (1.389 g, 86% yield). The as-prepared catalytic material was characterized by FTIR, ICP-AES, PXRD, TGA, XPS and TEM.

Synthesis of supported nickel nanoparticles stabilized by quinine on unfunctionalized halloysite (NiNP-QN@HAL). A Fisher-Porter bottle was charged with bis(cyclooctadiene)nickel(0) (343.0 mg, 1.25 mmol), quinine (QN: 371.0 mg, 1.15 mmol) and halloysite (1500 mg, 5.10 mmol), and then sealed with a septum inside the glovebox. The Fisher-Porter bottle was then removed from the glovebox and the solids were suspended in degassed EtOH (50 mL) under Ar prior to sealing the Fisher-Porter with its head. The system was then pressurized with H_2 (3 bar) at room temperature, heated at 100 °C and stirred for 18 h. A black dispersion was obtained and this suspension was then transferred to a centrifuge tube under Ar. Centrifugation was carried out at 3000 rpm for 5 min. After removal of the supernatant, the solid was dispersed in degassed EtOH (3× 10 mL). The obtained black solid was dried under vacuum overnight and stored in the glovebox (1.369 g, 75% yield). The as-prepared catalytic material was characterized by FTIR, ICP-AES, PXRD, TGA, XPS and TEM.

General procedure for Ni-catalyzed hydrogenation reactions at low pressure. Substrate (1.0 mmol) in 1 mL of EtOH (except on the case of *E*-alkenes were CPME was used as solvent) and in the

presence of the Ni corresponding catalytic material (from 1 to 5 mol%: NiNP/quinidine@HAL, NiNP/quinine@HAL, NiNP@HAL-NEt_3, NiNP@HAL-NH_2) was pressurized with H_2 at room temperature (3 bar) in a Fisher-Porter bottle, heated at the specified temperature and stirred for the appropriate time. After depressurization and cooling down to room temperature (when needed), the organic phase was recovered by filtration and the catalytic material was washed with pentane (3×2 mL). The combined organic fractions were analyzed by Gas Chromatography coupled with a Mass Spectrometry detector, using 2-methoxynaphtalene as internal standard, unless otherwise stated.

General procedure for Ni-catalyzed hydrogenation reactions at high pressure. The substrate (1.0 mmol of fatty acids or 0.5 mmol of squalene) in the presence of the corresponding Ni catalyst (from 5 to 20 mol%) was pressurized with H_2 (from 10 to 40 bar) at room temperature and heated at the specified temperature, and stirred for the appropriate time, using a high-pressure autoclave. After depressurization and cooling down to room temperature, the product and the catalyst were washed with pentane (3×2 mL) and the product was recovered after filtration through Celite®. The combined pentane fractions were evaporated under reduced pressure and the organic residue was analyzed by ^{1}H NMR (except for squalene which was analyzed by GC-FID), using dimethyl sulfone as internal standard.

Acknowledgements

A. P. A., S. M., D. P., and M. G. thank the Université Toulouse 3 – Paul Sabatier, the Centre National de la Recherche Scientifique (CNRS), and IMT Mines Albi for their financial support. A. P. A. thanks the Université Fédérale de Toulouse and Région Occitanie for his doctoral fellowship (APR2019-CATPROC). The authors also acknowledge Sonia Mallet-Ladeira, Christian Pradel, and Yannick Coppel for their helpful discussions on PXRD, (HR)-TEM, and solid state NMR analyses, respectively.

Conflict of Interest

The authors declare no conflict of interest.

Data Availability Statement

The data that support the findings of this study are available from the corresponding author upon reasonable request.

Keywords: biomass-based compounds · catalytic hydrogenation · halloysite · nickel nanoparticles

[1] A. Ito, R. Wagai, *Sci. Data* **2017**, *4*, 170103.
[2] a) G. Nagendrappa, *Appl. Clay Sci.* **2011**, *53*, 106; b) G. Nagendrappa, R. R. Chowreddy, *Catal. Surv. Asia* **2021**, *25*, 231.
[3] a) E. Joussein, S. Petit, J. Churchman, B. Theng, D. Righi, B. Delvaux, *Clay Miner.* **2005**, *40*, 383; b) Y. Lvov, W. Wang, L. Zhang, R. Fakhrullin, *Adv. Mater.* **2016**, *28*, 1227; c) P. Yuan, D. Tan, F. Annabi-Bergaya, *Appl. Clay Sci.* **2015**, *112–113*, 75.
[4] G. Cavallaro, G. Lazzara, S. Milioto, F. Parisi, *Chem. Rec.* **2018**, *18*, 940.
[5] a) M. Massaro, C. G. Colletti, G. Lazzara, S. Milioto, R. Noto, S. Riela, *J. Mater. Chem. A* **2017**, *5*, 13276; b) S. Sadjadi, *Appl. Clay Sci.* **2020**, *189*, 105537.
[6] A. Y. Sidorenko, A. V. Kravtsova, I. V. Il'ina, J. Warna, D. V. Korchagina, Y. V. Gatilov, K. P. Volcho, N. F. Salakhutdinov, D. Y. Murzin, V. E. Agabekov, *J. Catal.* **2019**, *380*, 145.
[7] J. Hamdi, B. N. Diehl, K. Kilgore, S. A. Lomenzo, M. L. Trudell, *ACS Omega* **2019**, *4*, 19437.
[8] Y. Zhang, X. He, J. Ouyang, H. Yang, *Sci. Rep.* **2013**, *3*, 2948.
[9] M. Massaro, R. Noto, S. Riela, *Catalysts* **2022**, *12*, 149.
[10] A. Philip, J. Lihavainen, M. Keinanen, T. T. Pakkanen, *Appl. Clay Sci.* **2017**, *143*, 80.
[11] Y. H. Ahmad, A. T. Mohamed, K. A. Mahmoud, A. S. Aljaber, S. Y. Al-Qaradawi, *RSC Adv.* **2019**, *9*, 32928.
[12] a) J. E. Jaine, M. R. Mucalo, *Mater. Res. Bull.* **2019**, *111*, 251; b) V. Vinokurov, A. Glotov, Y. Chudakov, A. Stavitskaya, E. Ivanov, P. Gushchin, A. Zolotukhina, A. Maximov, E. Karakhanov, Y. Lvov, *Ind. Eng. Chem. Res.* **2017**, *56*, 14043; c) S. Sadjadi, M. Akbari, E. Monflier, M. M. Heravi, B. Leger, *New J. Chem.* **2018**, *42*, 15733; d) S. Sadjadi, F. Koohestani, G. Pareras, M. Nekoomanesh-Haghighi, N. Bahri-Laleh, A. Poater, *J. Mol. Liq.* **2021**, *331*, 115740.
[13] Z. Zhu, D. Ding, Y. Zhang, Y. Zhang, *Appl. Clay Sci.* **2020**, *196*, 105761.
[14] a) I. K. Tonle, T. Diaco, E. Ngameni, C. Detellier, *Chem. Mater.* **2007**, *19*, 6629; b) P. Yuan, P. D. Southon, Z. Liu, M. E. R. Green, J. M. Hook, S. J. Antill, C. J. Kepert, *J. Phys. Chem. C* **2008**, *112*, 15742.
[15] a) S. Jansat, M. Gomez, K. Philippot, G. Muller, E. Guiu, C. Claver, S. Castillon, B. Chaudret, *J. Am. Chem. Soc.* **2004**, *126*, 1592; b) F. Chahdoura, C. Pradel, M. Gómez, *Adv. Synth. Catal.* **2013**, *355*, 3648; c) M. Rodríguez-Rodríguez, P. Llanes, C. Pradel, M. A. Pericàs, M. Gómez, *Chem. Eur. J.* **2016**, *22*, 18247; d) E. Raluy, I. Favier, A. M. Lopez-Vinasco, C. Pradel, E. Martin, D. Madec, E. Teuma, M. Gomez, *Phys. Chem. Chem. Phys.* **2011**, *13*, 13579; e) I. Favier, M.-L. Toro, P. Lecante, D. Pla, M. Gómez, *Catal. Sci. Technol.* **2018**, *8*, 4766; f) T. A. G. Duarte, I. Favier, C. Pradel, L. M. D. R. S. Martins, A. P. Carvalho, D. Pla, M. Gómez, *ChemCatChem* **2020**, *12*, 2295 ; g) G. Garg, S. Foltran, I. Favier, D. Pla, Y. Medina-González, M. Gómez, *Catal. Today* **2020**, *346*, 69; h) I. Favier, D. Pla, M. Gómez, *Chem. Rev.* **2020**, *120*, 1146.
[16] a) A. Reina, I. Favier, C. Pradel, M. Gómez, *Adv. Synth. Catal.* **2018**, *360*, 3544; b) A. Reina, C. Pradel, E. Martin, E. Teuma, M. Gómez, *RSC Adv.* **2016**, *6*, 93205; c) A. Reina, A. Serrano-Maldonado, E. Teuma, E. Martin, M. Gómez, *Catal. Commun.* **2018**, *104*, 22.
[17] a) M. C. Biesinger, B. P. Payne, L. W. M. Lau, A. Gerson, R. S. C. Smart, *Surf. Interface Anal.* **2009**, *41*, 324; b) M. C. Biesinger, L. W. Lau, A. R. Gerson, R. S. C. Smart, *Phys. Chem. Chem. Phys.* **2012**, *14*, 2434.
[18] A. Reina, C. Pradel, E. Martin, E. Teuma, M. Gomez, *RSC Adv.* **2016**, *6*, 93205.
[19] a) A. Vargas, A. Baiker, *J. Catal.* **2006**, *239*, 220; b) S. Noel, E. Caronia, H. Bricout, I. C. Ticha, S. Menuel, A. Ponchel, S. Tilloy, A. Galia, E. Monflier, J. Jindrich, B. Leger, *Catal. Commun.* **2021**, *150*, 106272.
[20] D. Sanhes, E. Raluy, S. Rétory, N. Saffon, E. Teuma, M. Gómez, *Dalton Trans.* **2010**, *39*, 9719.
[21] S. M. Silva, A. F. Peixoto, C. Freire, *Appl. Catal. A* **2018**, *568*, 221.
[22] a) I. Favier, S. Massou, E. Teuma, K. Philippot, B. Chaudret, M. Gómez, *Chem. Commun.* **2008**, 3296; b) I. Favier, P. Lavedan, S. Massou, E. Teuma, K. Philippot, B. Chaudret, M. Gomez, *Top. Catal.* **2013**, *56*, 1253; c) S. Losse, H. Junge, *ChemSusChem* **2010**, *3*, 1409.
[23] D. Tichit, F. Medina, R. Durand, C. Mateo, B. Coq, J. E. Sueiras, P. Salagre, in *Studies in Surface Science and Catalysis, Vol. 108* (Eds.: H. U. Blaser, A. Baiker, R. Prins), Elsevier, **1997**, pp. 297.
[24] S. Noel, D. Bourbiaux, N. Tabary, A. Ponchel, B. Martel, E. Monflier, B. Leger, *Catal. Sci. Technol.* **2017**, *7*, 5982.
[25] R. Ciriminna, V. Pandarus, F. Beland, M. Pagliaro, *Org. Process Res. Dev.* **2014**, *18*, 1110.
[26] a) Y. Wang, D. Zhao, D. Rodriguez-Padron, C. Len, *Catalysts* **2019**, *9*, 28558; b) X. Chen, L. Zhang, B. Zhang, X. Guo, X. Mu, *Sci. Rep.* **2016**, *6*.
[27] a) X. Huang, K. Liu, W. L. Vrijburg, X. Ouyang, A. Iulian Dugulan, Y. Liu, M. W. G. M. Tiny Verhoeven, N. A. Kosinov, E. A. Pidko, E. J. M. Hensen, *Appl. Catal. B* **2020**, *278*, 119314; b) H. C. Genuino, H. H. van de Bovenkamp, E. Wilbers, J. G. M. Winkelman, A. Goryachev, J. P. Hofmann, E. J. M. Hensen, B. M. Weckhuysen, P. C. A. Bruijnincx, H. J. Heeres, *ACS Sustainable Chem. Eng.* **2020**, *8*, 5903.
[28] a) A. Patti, H. Lecocq, A. Serghei, D. Acierno, P. Cassagnau, *J. Ind. Eng. Chem.* **2021**, *96*, 1; b) A. Mortensen, F. Aguilar, R. Crebelli, A. Di Domenico, B. Dusemund, M. J. Frutos, P. Galtier, D. Gott, U. Gundert-Remy, J.-C. Leblanc, O. Lindtner, P. Moldeus, P. Mosesso, D.

Parent-Massin, A. Oskarsson, I. Stankovic, I. Waalkens-Berendsen, R. A. Woutersen, M. Wright, M. Younes, P. Boon, D. Chrysafidis, R. Guertler, P. Tobback, P. Gergelova, A. M. Rincon, C. Lambre, *EFSA J.* **2017**, *15*, 4785.
[29] S.-K. Kim, F. Karadeniz, *Adv. Food Nutr. Res.* **2012**, *65*, 223.
[30] V. Pandarus, R. Ciriminna, F. Beland, M. Pagliaro, S. Kaliaguine, *ACS Omega* **2017**, *2*, 3989.
[31] R. Mariscal, P. Maireles-Torres, M. Ojeda, I. Sadaba, M. Lopez Granados, *Energy Environ. Sci.* **2016**, *9*, 1144.
[32] Y. Xu, S. Qiu, J. Long, C. Wang, J. Chang, J. Tan, Q. Liu, L. Ma, T. Wang, Q. Zhang, *RSC Adv.* **2015**, *5*, 91190.
[33] a) G. C. Hayes, C. R. Becer, *Polym. Chem.* **2020**, *11*, 4068; b) S. Dutta, N. S. Bhat, *ChemCatChem* **2021**, *13*, 3202.
[34] F. Ferlin, F. Valentini, A. Marrocchi, L. Vaccaro, *ACS Sustainable Chem. Eng.* **2021**, *9*, 9604.
[35] a) Z. Zhang, *ChemSusChem* **2016**, *9*, 156; b) Z. Yu, X. Lu, J. Xiong, X. Li, H. Bai, N. Ji, *ChemSusChem* **2020**, *13*, 2916.

Manuscript received: June 20, 2022
Revised manuscript received: August 31, 2022
Accepted manuscript online: September 6, 2022
Version of record online: ■■, ■■■

RESEARCH ARTICLE

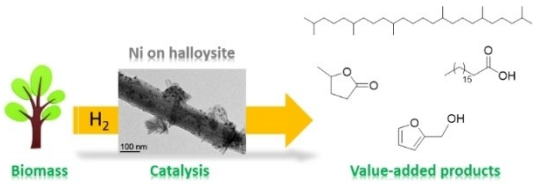

A. Pérez Alonso, S. Mauriés, J.-B. Ledeuil, Dr. L. Madec, Prof. D. Pham Minh, Dr. D. Pla, Prof. M. Gómez**

1 – 10

Nickel Nanoparticles Immobilized on Pristine Halloysite: An Outstanding Catalyst for Hydrogenation Processes

A sustainable nanomaterial: The partnership between a nanoclay (halloysite) and a first-row transition metal (nickel) led to a versatile catalyst, permitting the synthesis of target products by hydrogenation processes, together with a remarkable selectivity and an efficient catalyst recycling.